

Highlighting the Role of the Medium in DFT Analysis of the Photophysical Properties of Ruthenium(II) Polypyridine-Type Complexes

Marie-France Charlot*^{*,†} and Ally Aukauloo*^{*,†,‡}

Laboratoire de Chimie Inorganique, Institut de Chimie Moléculaire et des Matériaux d'Orsay
UMR CNRS 8182, Université Paris-Sud, 91405 Orsay Cedex, France, and iBiTec-S,
CEA Saclay, Bât. 532, 91191 Gif-sur-Yvette Cedex, France

Received: June 14, 2007; In Final Form: August 23, 2007

In order to test the pertinence of the density functional theory to interpret the photophysical properties of ruthenium(II) polypyridine-type complexes, DFT and TDDFT calculations are performed both on the isolated molecule and in solution media described by the dielectric-like polarized continuum model (PCM). This study is focused on three isoelectronic complexes: $[\text{Ru}(\text{bpy})_2(\text{PhenImHPh})]^{2+}$ (**II**), where PhenImHPh represents the 2-(3,5-ditertbutylphenyl)imidazo[4,5-f][1,10]phenanthroline ligand, as well as $[\text{Ru}(\text{bpy})_2(\text{PhenImPh})]^+$ (**I**), and $[\text{Ru}(\text{bpy})_2(\text{PhenImH}_2\text{Ph})]^{3+}$ (**III**), obtained by changing the protonic state of the imidazole ring. The structural and electronic properties of the ground and lowest triplet states are fully characterized in vacuo and in water solution, and the absorption spectra in the visible region are also investigated by TDDFT. The theoretical data are compared to the electrochemistry, UV–visible, and photophysical experiments to assess the validity and limits of each type of calculation. The choice of the functional is also discussed.

Introduction

The ruthenium(II) polypyridyl-type complex is a unique class of robust coordination metal compounds with remarkable photophysical properties that are likely to be used in technical applications for the capture and conversion of light energy. Thus, it is important to clarify their electronic structure and to assign correctly their low-lying electronic states for a better understanding of both energy- and electron-transfer pathways. Density functional theory (DFT) and time-dependent DFT (TDDFT) calculations are techniques now widely used to describe the ground and excited electronic states of d^6 transition-metal complexes and to interpret a large panel of their properties (see, for instance, ref 1 and references therein).

Charge transfers are the key phenomena involved in the absorption and emission properties of these compounds. These transitions lead to substantial changes in the electronic distribution between the initial and final states. Photophysical studies of these complexes are generally carried out in water, that is, in a polar medium; therefore, the solvent molecules will respond to these modifications. A number of recent reports have emphasized the importance of including the surroundings in computations.^{2–5} This has namely been taken into account for the description of the UV–vis spectra where only the singlet excited states are computed. More tempting is the description of the photophysical properties, whereby an increasing interest is devoted to the calculation of the triplet states. Consequently, an enormous computation effort is necessary to introduce the surroundings into these open-shell calculations,^{6,7} especially for large $[\text{M}(\text{bpy})_2\text{L}]^{2+}$ -type complexes with a substituted bipyridine or phenanthroline including more than 80 atoms.⁸ It becomes therefore crucial to critically assess the applicability of DFT

techniques to gain the ground- and excited-state properties of these complexes. As such calculations are highly memory- and time-demanding, it is, in our opinion, suitable to infer in which case an alleviation could be made without drastic alteration of the conclusions.

In a previous paper,⁹ based on DFT calculations, we were recently able to interpret the unusual photophysical properties of a complex $[(\text{bpy})_2\text{Ru}(\text{LH}_2)]^{2+}$, where LH_2 is the heteroditopic ligand *N,N'*-bis(3,5-di-*tert*-butylsalicylidene)-5,6-(1,10-phenanthroline) diamine, which can be considered as a fused phenanthroline and a tetradentate Schiff base cavity. Indeed, TDDFT calculations allowed us to underpin the role of a spectroscopically silent but photophysically important triplet excited state in the occurrence of a rapid quenching of emission. Of note, such a conclusion was obtained on the isolated molecule. In a more recent study,⁸ however, such a calculating method in absence of surroundings has proven to be unrealistic for a family of complexes. This work deals with the influence of the protonic states of the imidazole ring on both the ground- and excited-states properties of a complex $[\text{Ru}(\text{bpy})_2(\text{PhenImHPh})]^{2+}$ (**II**), where PhenImHPh stands for 2-[(3',5'-di-*tert*-butylbenzene)]-imidazo[4,5-f]^{1,10}-phenanthroline.

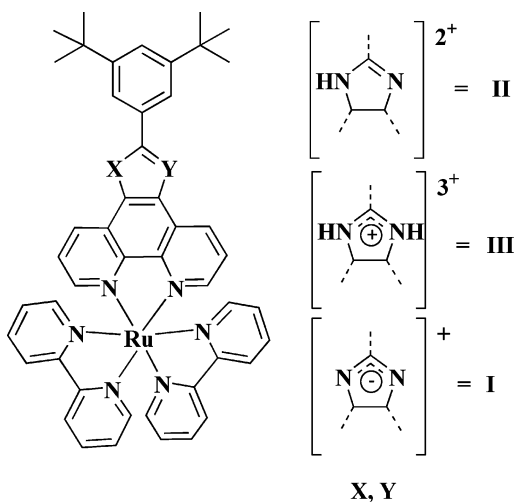
In the present paper, we will detail the points which constrained us to achieve much more consuming calculations in the presence of a solvent. This study concerns complex (**II**) along with the $[\text{Ru}(\text{bpy})_2(\text{PhenImPh})]^+$ (**I**) and $[\text{Ru}(\text{bpy})_2(\text{PhenImH}_2\text{Ph})]^{3+}$ (**III**) derivatives, where in the first case, the secondary amino group is in the deprotonated state, while in the second case, the imino nitrogen of the imidazole ring is protonated (see Chart 1). We will compare the conclusions that can issue from DFT and TDDFT results on the isolated molecule (calculation in vacuo) and in a condensed phase (calculation in a modeled solvent). In doing so, we hope that general trends will emerge and help for future studies. We restrict the study to large Ru polypyridine complexes which are synthesized and characterized in our laboratory^{10–12} and focus essentially on their

* To whom correspondence should be addressed. E-mail: mcharlot@icmo.u-psud.fr (M.-F.C.); aukauloo@icmo.u-psud.fr (A.A.).

[†] Université Paris-Sud.

[‡] CEA Saclay.

CHART 1



photophysical properties. The calculations of triplet states and the oxidized forms therefore represent an important part of this work. Our final goal is to draw some general conclusions to tune the chain of calculations for future work on systems of increasing size and complexity. We also report a limited study of singlet states which serves only as criterion of the computation quality; it is thought that a reasonable agreement between a calculated and experimental visible spectrum is a good starting point for the validation of the method.

Experimental Section

Density functional theory calculations were carried out using Becke's three-parameter hybrid functional B3LYP,^{13,14} along with the valence double- ζ basis set LanL2DZ^{15,16} including the Los Alamos effective core potential for heavy atoms. All calculations were performed using the Gaussian 03¹⁷ software package. For consistency reasons, we did not use experimental structures but calculated geometries which were fully optimized for the three isolated molecules in their ground state (closed-shell singlet S_0). However, in order to decrease the computation time, the two *tert*-butyl (*t*Bu) groups on the phenyl ring, which present numerous degrees of freedom without influence on our problem, were replaced by two methyl groups. Starting from the closed-shell S_0 state, time-dependent density functional calculations (TDDFT)¹⁸ were performed to determine the energies and character of the lowest excited singlet and triplet states in the ground-state geometry. As photophysical experiments, in the absence as well as in the presence of an electron acceptor, may involve the lowest triplet state T_1 and the ground doublet state D_0 of the oxidized complex, these two states were completely studied using a different approach; spin-unrestricted calculations were performed, and the corresponding geometries of T_1 and D_0 were fully optimized in vacuo at the UB3LYP/LanL2DZ level, except for the oxidized form of **III**, a highly charged (+4) complex for which convergence of the geometry optimization was not achieved. We have checked that, in the open-shell calculations, the spin contamination from states of higher spin multiplicity is low by looking at the values of $\langle S^2 \rangle$ (2.020 in **I**, 2.006 in **II**, and 2.010 for **III** in vacuo T_1 states). The nature of these states was explained by analysis of the corresponding spin-orbitals and spin density distributions, as done by other authors.³

In a first step, all of our study concerned the isolated molecule (in vacuo calculations). In a second step, solvent effects were modeled in the framework of a self-consistent reaction field

method (SCRf) based on the important class of continuum models,¹⁹ which make use of the laws of standard electrostatics. These calculations were performed with the integral equation formalism (IEF) version^{20,21} of the dielectric-like polarizable continuum model (PCM).²² They concerned the geometries optimized in vacuo and took into account the changes of formalism²³ implemented in the recent version of Gaussian 03. The time-dependent DFT results involving two different electronic states are, by default, nonequilibrium calculations with respect to the polarization process between the solvent reaction field and the charge density of the solute.²⁴ All calculations were hence repeated in water. This choice was guided by the fact that all of the photophysical experiments, which constitute the key point of our study, were realized in an aqueous medium. However, as the guiding line of this study deals with the solvation effects, we also performed selected calculations in solvents of different polarity, dichloromethane, acetonitrile, and methanol. The reasons behind will be explained in the following sections.

Parameters of the model defining the shape of the solvent cavity and description of the solvent were kept to their default value as implemented in the D.02 revision of Gaussian 03,¹⁷ except one. By default, the cavity is defined by putting a sphere around each solute heavy atom, and hydrogen atoms are enclosed in the sphere of the atom to which they are bonded. However, hydrogens bonded to atoms like N or O may have a marked acidic character, and it is possible to add an individual sphere on them. We tested this modification and included spheres on the H atoms on the imidazole ring (1 in **II** and 2 in **III**). The interaction between the polarized solute and the solvent, the orbital energies, as well as the dipole moment changed by, at most, 2%, and the HOMO–LUMO energy gap changed by 0.2%. The total SCF energy after PCM correction was unaffected. This nonsignificant modification of the cavity is therefore not taken into account in the following results.

Geometry optimizations were not attempted in solvents. The main reason is that the studied complexes are very large molecules for which optimizations in the absence of surroundings are already difficult to achieve. This is especially true for the triplet states for which the loose optimization criterion has generally been used. For the oxidized form of complex **III** (**IIIox**), which bears a +4 charge, optimization has not converged, and this even on the isolated molecule.

UV–visible spectra were simulated by a sum of individual Gaussian line shapes with a value of 3200 cm^{-1} ($\sim 0.40 \text{ eV}$) for the full-width at half-maximum (fwhm) and a band area proportional to the calculated oscillator strength. Such a value of the fwhm is used in similar simulations.^{2,6}

Results

Optimized Geometries. As a prerequisite to all calculations, the optimized geometric parameters for the ground-state S_0 , the lowest triplet state T_1 , and the lowest D_0 doublet state of the oxidized form were calculated at the (U)B3LYP/LanL2DZ level for the three complexes (**I**, **II**, and **III**) in vacuo and reported for states S_0 and T_1 previously.⁸

Energy Levels and Molecular Orbitals in the Ground State. Complexes I, II, and III in Vacuo. For the isolated molecules, we choose first to describe the orbitals of **II**, which as mentioned before, can be considered as the parent compound for this study. The energies and preponderant compositions are listed in Table S1, and some typical MOs are presented in Figure 1. All descriptions and notations have been detailed elsewhere.⁹ The energy diagram (in atomic units, au) of the frontier orbitals of **II** is plotted in the middle part of Figure 2.

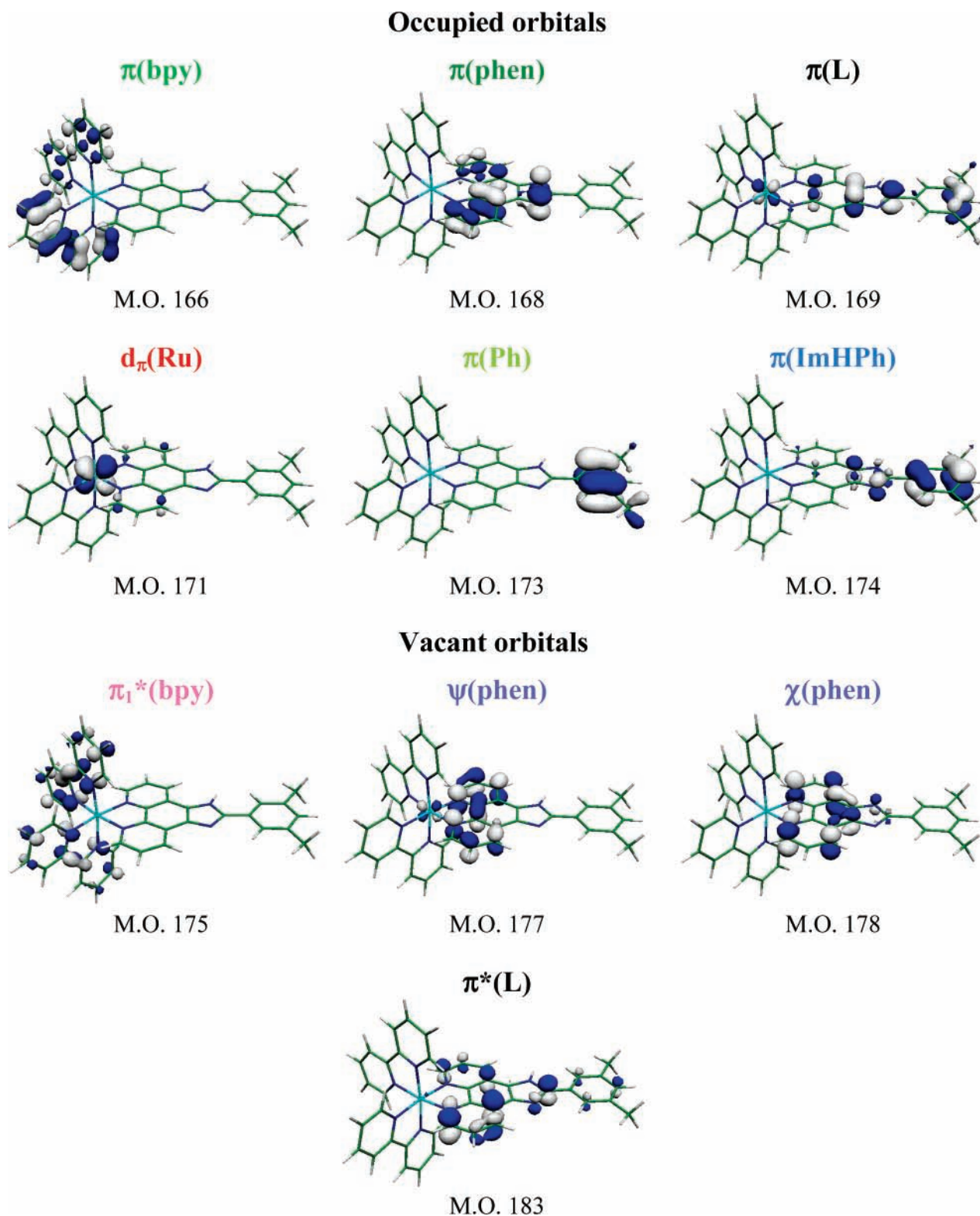


Figure 1. Selected orbitals calculated in vacuo for the ground-state S_0 of **II**. They define the orbital types.

The evolution of the ground-state MOs of the deprotonated **I** and protonated **III** complexes is described in comparison with compound **II**, and the correlation is established between the orbitals of the three complexes in Figure 2. The energies and preponderant compositions are listed in Tables S2 and S3 of the Supporting Information. The increasing total charge on the ruthenium complexes when going from **I** to **III** leads, in vacuo, to consequent energetic stabilization of all of the orbitals. In order to have a clearer visual comparison of the relative MOs energies in the three complexes, we make use of a mathematical

trick. A clear-cut fact is that the two combinations of the first vacant orbital π_1^* of the two bipyridines retain almost the same AO composition in the complexes **I**–**III**. Therefore, it seems judicious to proceed to an artificial leveling of these MOs by subtracting 0.073 au from all energies for **I** and by adding 0.070 au for **III** (see Figure 2). This is also supported by the experimental data concerning the reduction potential; it was reported that the two bipyridine fragments reduce at almost the same potentials in the three complexes, as evidenced by the two first half-wave reduction potentials in cyclic voltammetry.⁸

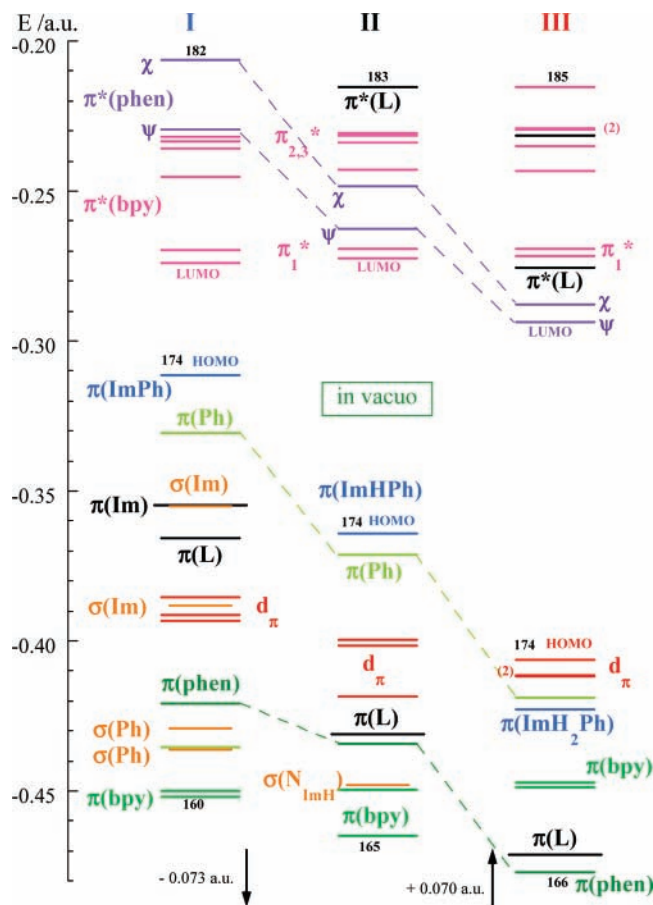


Figure 2. Energy level diagram (in atomic units, au) of frontier MOs for the ground-state S_0 of **I** (left), **II** (middle), and **III** (right) calculated in vacuo. The energy levels for **I** and **III** are shifted by -0.073 and $+0.070$ au, respectively, in order to account for the $+1$ and $+3$ charges of the complexes as compared to the $+2$ charge of the parent complex (see text). Correlations between orbitals of the same type are evidenced.

A striking fact from a mere comparison of the MO level diagram is the downshift in energy for all of the orbitals located on the ligand upon protonation. A selection of occupied π orbitals in the ground state of the three complexes developed within the imidazole region or on the whole ligand are indicated in Figure 3.

Our computed Mulliken charges (Table 1) on each fragment for the three complexes indicate that the ruthenium ion retains almost the same charge, that is, 0.887 in **I**, 0.892 in **II**, and 0.895 in **III**, and the charge on each bipyridine ligand increases by only 0.077 as the total charge increases by 1 upon going from **I** to **II** to **III**. In contrast, strong variations of the charge on the imidazole-containing ligand are observed, about 0.4 on the phenanthroline moiety and also 0.4 on the imidazole phenyl part. This expresses that upon protonation or deprotonation of the ligand L, the variation of charge is not delocalized on the whole complex and that important charge gradients between the different parts of the molecule are generated.

Continuing our analysis of Figure 2, we see that the mean difference in energy between the set of d_{π} orbitals and the LUMO is nearly the same, that is, 3.18, 3.65, and 3.16 eV for **I**, **II**, and **III**, respectively, in comparison to 3.56 eV calculated for $[\text{Ru}(\text{bpy})_3]^{2+}$.⁹ In contrast, it is relevant to note that the HOMO–LUMO energy gap increases substantially with the positive charge from 1.02 eV in **I** to 2.50 eV in **II** and 3.07 eV in **III**. The exceedingly low value for the deprotonated complex, which presents an enhanced electron density on the imidazole ring, results from an unrealistic destabilization of the orbitals

located on this part of the molecule. Consequently, the energies of the excited states calculated in vacuo will be strongly underestimated.

Influence of a Medium of Increasing Polarity. Our primary target is to understand the influence of the surroundings on the calculated molecular orbital levels of each complex. As the computed data in vacuo for complex **I** seem physically meaningless, we choose this compound to investigate the effects and further compare the results in different media, vacuum, dichloromethane with a low dielectric constant $\epsilon = 8.93$, and water, a highly polar solvent ($\epsilon = 78.39$). The telling fact is that as the polarity of the medium rises, the interaction between the $+1$ charged molecule and the solvent rises. A more effective charge separation is favored, as reflected by the increase in dipole moment from 26.6 D in vacuo to 35.2 D in CH_2Cl_2 and 36.8 D in H_2O (see Table 2). Such a trend is in accord with previous reports.²⁵ The solvation energy (electrostatic polarized solute–solvent energy) amounts to -66 kcal/mol in CH_2Cl_2 and -81 kcal/mol in H_2O , inferring that the solvated complex is stabilized in polar solvents. Another clear outcome is that all MO levels are not effected in the same way. Figure 4 evidences that the first two unoccupied orbitals which are developed on the bipyridines are destabilized in solvents relative to in vacuo so that a shift of -0.093 au in CH_2Cl_2 and -0.106 au in H_2O is necessary to align them on the same energy. This artificial leveling points out clearly (Figure 4) that in solvents of increasing polarity, all orbitals localized on the ligand L are more and more stabilized compared to those on ruthenium or bipyridine. This is especially true for orbitals developed on the imidazole phenyl part, that is, on the more electron-rich fragment of the complex. Two consequences follow. (i) In solution, only one orbital lies higher in energy than the ruthenium d_{π} orbitals instead of five calculated in vacuo. This point will highly influence the nature of the low-lying excited states. (ii) The HOMO–LUMO energy gap increases enormously from 1.02 (vacuo) to 2.54 (CH_2Cl_2) and 2.84 eV (H_2O). A consequence of this fact is that no excited state will be calculated at low energy.

The role of the surroundings can be evidenced for compounds **I** and **III** on the corresponding MO energy level diagrams presented in the Supporting Information (Figures S1 and S2, respectively). The orbital energies and characters are reported in Tables S1–S3, and comparison of some molecular properties in different media is gathered in Table 2. For complex **II**, holding an imidazole in its normal protonation state, the HOMO–LUMO gap also increases in solvents. The orbitals located on the ligand L are also more stabilized compared to those on ruthenium or bipyridine, although this phenomenon is less pronounced than that for **I**. In water, the highest orbital developed on the imidazole phenyl part drops down in the energy range of the ruthenium orbitals and consequently mixes with one of the d_{π} orbitals. The calculated HOMO is now a d_{π} orbital.

For complex **III** in the three media, MOs on the protonated imidazole phenyl part retain almost the same energy, while the phen orbitals are slightly more destabilized than the bpy orbitals. The dipole moment, which was already small in vacuo, is only slightly effected as well as the HOMO–LUMO gap. This latter point allows one to anticipate that, for this compound, the calculated excited states for the isolated molecule and in solution will not differ drastically.

Complexes I, II, and III in H_2O Medium. A diagram of correlation between the orbital energy levels of the three complexes in water is reported in Figure 5 and has to be

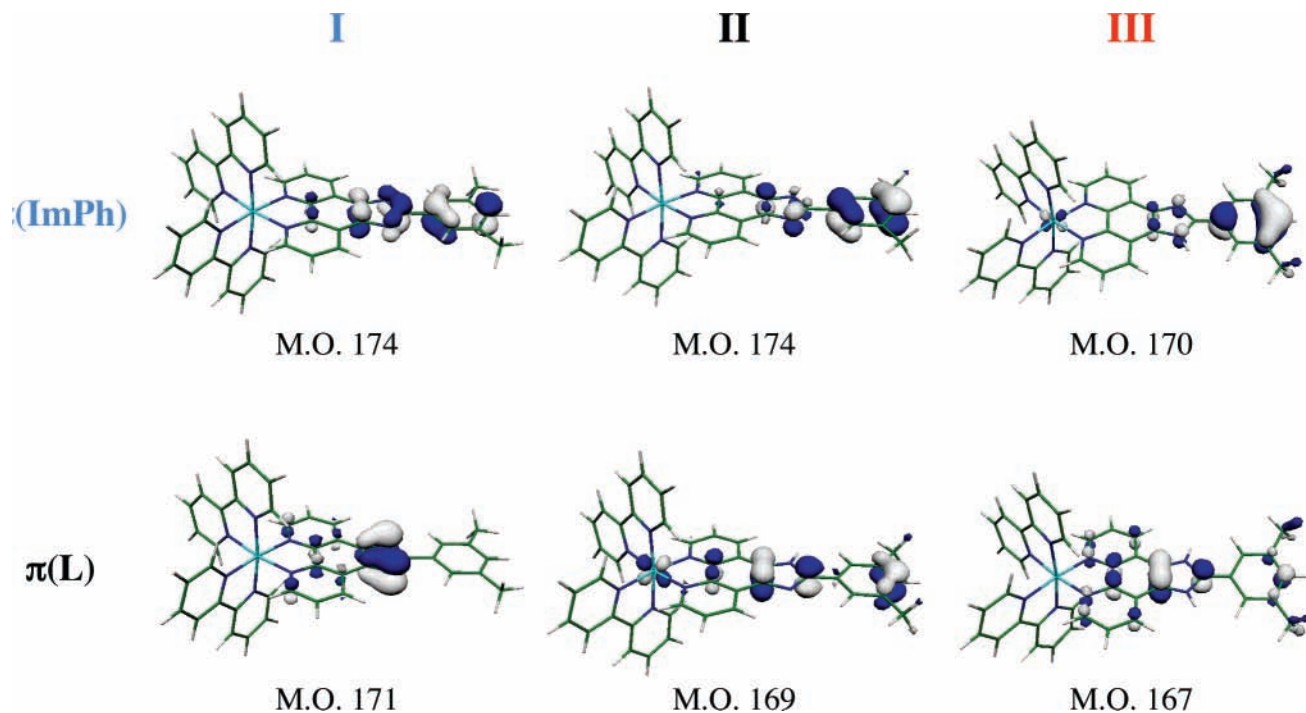


Figure 3. Selected orbitals developed in the imidazole region calculated in vacuo for the ground-state S_0 of the three complexes.

TABLE 1: Mulliken Charges for Different Fragments of Complexes I, II, and III as well as for $[\text{Ru}(\text{bpy})_3]^{2+}$ (Ru-bp) Calculated in Three Surroundings, Vacuum and Two Solvents (CH_2Cl_2 and H_2O); Molecular Charges are Given in Parentheses

complex	fragment	vacuum	CH_2Cl_2	H_2O
Ru-bp (+2)	Ru	0.891	0.891	0.892
	bpy	0.370	0.370	0.370
I (+1)	Ru	0.887	0.890	0.892
	bpy1	0.273	0.331	0.343
	bpy2	0.273	0.331	0.343
	phen ^a	-0.265	-0.203	-0.186
	N(N)C-Ph	-0.167	-0.350	-0.391
II (+2)	Ru	0.892	0.895	0.896
	bpy1	0.349	0.364	0.366
	bpy2	0.352	0.366	0.367
	phen ^a	0.219	0.270	0.297
	NH(N)C-Ph	0.188	0.106	0.074
III (+3)	Ru	0.895	0.897	0.898
	bpy1	0.427	0.400	0.391
	bpy2	0.427	0.400	0.390
	phen ^a	0.600	0.657	0.671
	NH(NH)C-Ph	0.650	0.646	0.651

^a The phen stands for the phenanthroline part of ligand L.

compared to Figure 2 for the same complexes in vacuo. The first concluding remark is that no leveling of the energies was necessary when correlating the three complexes. Another striking evidence is that occupied, as well as vacant, orbitals on the bipyridine have the same energies in the three complexes. Turning our attention to the Mulliken charges on different fragments of the complexes (Table 1), we note that while the bpy ligands accumulate an increasing amount of positive charge upon protonation of the imidazole ring in vacuo, their charge remains almost constant in water. Ruthenium d_{π} orbitals are slightly stabilized upon going from deprotonated to normal and protonated imidazole due to the feeble increase of positive charge on the metal (Table 1).

Thus, in a polar solvent, orbitals developed on an identical nuclear fragment in different molecules tend to retain the same electronic density, conferring them with the same energy. We can tentatively relate this computed data to the experimental

TABLE 2: Dipole Moment μ , Electrostatic Solvation Energy between a Polar Solute and Solvent E_{solv} , and the HOMO-LUMO Energy Gap δ for Complexes I, II, and III as Well as for $[\text{Ru}(\text{bpy})_3]^{2+}$ (Ru-bp) Calculated in Three Surroundings, Vacuum and Two Solvents (CH_2Cl_2 and H_2O)

complex		vacuum $\epsilon = 1$	CH_2Cl_2 $\epsilon = 8.93$	H_2O $\epsilon = 78.39$
Ru-bp	μ (D)	0	0	0
	E_{solv} (kcal/mol)	0	-114	-130
	δ (eV)	3.363	3.348	3.338
I	μ (D)	26.6	35.2	36.8
	E_{solv} (kcal/mol)	0	-66	-81
	δ (eV)	1.020	2.541	2.842
II	μ (D)	11.9	16.5	17.4
	E_{solv} (kcal/mol)	0	-116	-136
	δ (eV)	2.500	3.338	3.361
III	μ (D)	-4.8 ^a	-3.8 ^a	-3.8 ^a
	E_{solv} (kcal/mol)	0	-232	-269
	δ (eV)	3.066	3.235	3.284

^a Dipole moment nearly along the pseudo C_2 axis but, in the other sense, as compared to I and II.

cathodic redox behavior of I, II, and III, where no significant change in potential is observed for the reduction waves for the three complexes. However, one must be aware that the calculation of the redox potential is not so trivial. The same reasoning holds for the experimental anodic behavior, where the $\text{Ru}^{\text{II}}/\text{Ru}^{\text{III}}$ oxidation potential is only slightly lower in I than that in II and III.⁸ In contrast, all orbitals developed on ligand L become more and more stabilized upon going from I to II to III, that is, upon increasing the (positive) nuclear charge on this part of the molecule. This stabilization is, however, considerably less pronounced in solution than that in vacuo, even if the increase of positive charge on L is more important (Table 1).

Excited Singlet States and Electronic Absorption Spectra. The low-lying singlet excited states of the three complexes in their ground-state geometry are studied using time-dependent DFT (TDDFT) calculations, a method which describes these states in terms of monoexcitations from occupied to vacant MOs of the ground state. From the computed data, we will compare results on the isolated molecule and in solvents. We have

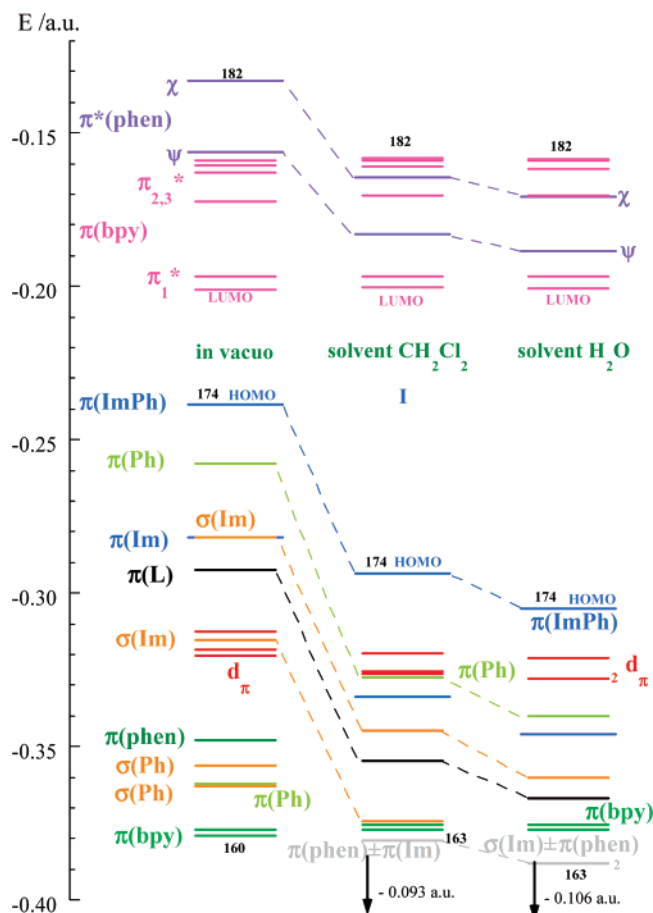


Figure 4. Energy level diagram (in au) of the ground-state MOs for compound **I**, calculated in vacuo, in CH_2Cl_2 and H_2O . The energy levels in CH_2Cl_2 and H_2O are shifted by -0.093 and -0.106 au, respectively, in order to level all of the π_1^* MOs (see text). Correlations between orbitals of the same type are evidenced.

theoretically tested the influence of different solvents (CH_2Cl_2 , CH_3OH , CH_3CN , and H_2O) on complexes **I**, **II**, and **III**. However, such an enterprise requires an important amount of computational means and does not constitute the final goal of our research. Therefore, we focus now on the behavior of complex **II** in vacuo and in water as a polar solvent and restrict to the energy domain including low-lying states and metal-to-ligand charge-transfer states.

Complex II in Vacuo. A given set of selected transitions to the singlet states of **II** in vacuo is described in Table S4 of the Supporting Information, and below, we sum up the main findings. Lying 2.18 eV above the ground state, state S_1 results essentially from a HOMO-to-LUMO monoexcitation. The corresponding transition at 569 nm is a ligand-to-bipyridine charge transfer, abbreviated as LBCT. The next transitions involve shifts of the electronic density from the HOMO developed on the imidazole phenyl part of the ligand to the vacant π orbitals of the phenanthroline moiety of the same ligand, that is, intraligand charge transfers (ILCT). On the ground-state absorption spectrum, they are seen as a shoulder, tailing up to 550 nm, on the more energetic MLCT band. To a first approximation, the states obtained by charge transfers from d_π to $\pi_1^*(\text{bpy})$ (referred to as MBCTs) or from d_π to $\psi(\text{phen})$ (MPCT transitions) result in different states ranging from 2.70 to 3.10 eV. They give rise to absorption between 440 and 400 nm. It is noteworthy that ILCT and LBCT transitions are computed in this region, with an oscillator strength of comparable magnitude.²⁶ Another key theoretical result is the intense

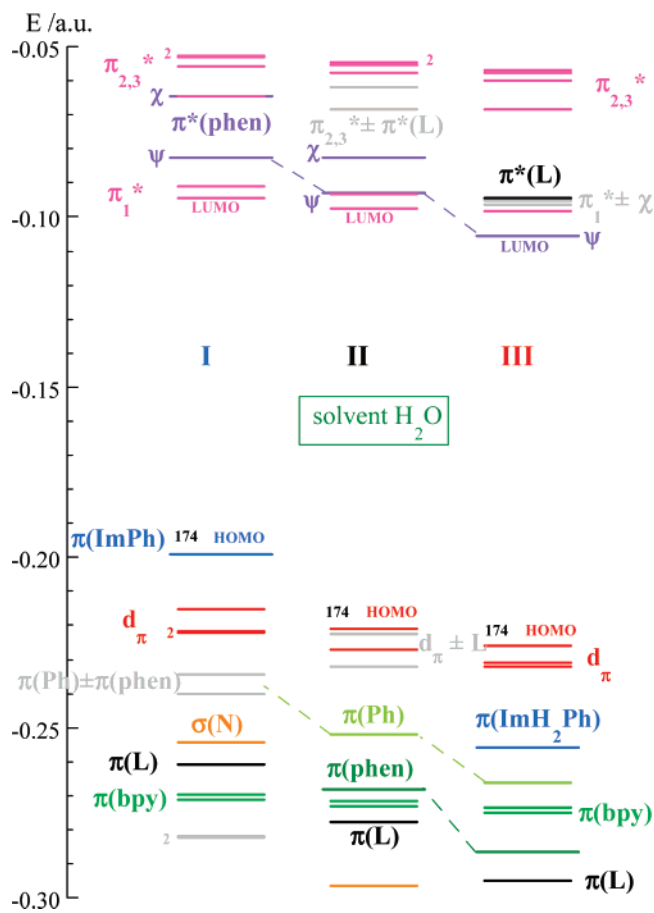


Figure 5. Energy level diagram (in au) of the ground-state MOs for compounds **I**, **II**, and **III** calculated in water. All energies are on the same scale without leveling.

absorption band ($f = 0.370$) calculated at 337 nm. This transition is obtained essentially by a monoexcitation from the HOMO developed on the imidazole phenyl part to MO 183 delocalized on the whole ligand (see Figure 1) and is therefore qualified as a π - π^* type localized on the ligand L.²⁷

Complex II in Aqueous Solution. The differences between in vacuo and solution for complex **II** are reported in Table S5 of the Supporting Information and can be visualized in Figure 6 for the region above 330 nm. The concluding remarks are as follows. (i) No transition is calculated in water above 500 nm, in agreement with the experimental spectrum (see the Supporting Information of ref 8). This fact contrasts with results in vacuo, where a band of low intensity is simulated around 550 nm. (ii) In solvent medium, the lowest energy transitions are all metal-to-bipyridine charge transfers. A comparison of the energy level diagrams of the ground-state MOs in vacuo (Figure 2) and in H_2O (Figure S1) reveals that the evolution of the spectra could be (at least qualitatively) predicted. The increase of the HOMO-LUMO gap shifts the transitions to a lower wavelength, and the energy drop of the two HOMOs located on L down the ruthenium orbitals is responsible for the MLCT type of the lowest energy transitions.

Both in vacuo as well as in solvent, a band is simulated around 440 nm with similar intensity. It is important to notice that in both surroundings, this band envelopes a mixture of metal-to-ligand charge transfers and intraligand charge transfers (ILCT) in ligand L with comparable contributions. This is not, as usually reported, a pure MLCT band. ILCTs involve electron transfers from the imidazole phenyl fragment toward the phenanthroline moiety. This fact is an important aspect in

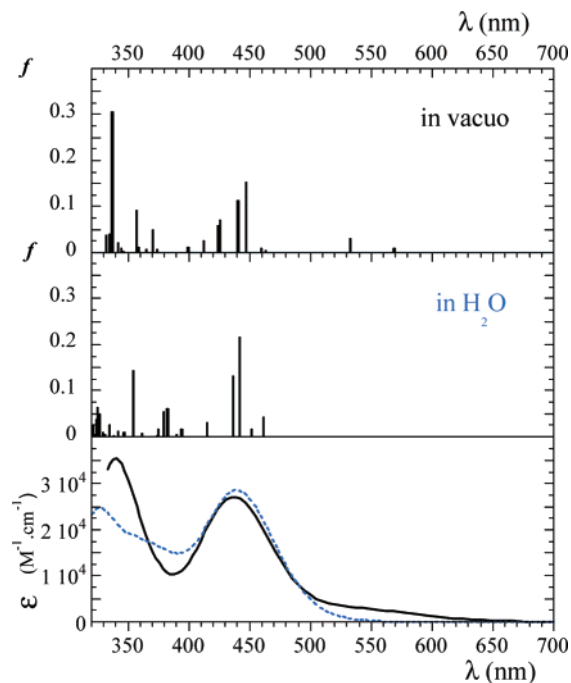


Figure 6. UV–visible spectrum of complex **II** above 330 nm. Calculated oscillator strengths in vacuo (top) and in H₂O (middle); simulated spectra (bottom) in vacuo (full line) and in H₂O (dashed line).

coordination chemistry, showing the effect of the metal in the electronic properties of the coordinated ligand.

Complexes I and III. The UV–visible spectra of complexes **I** and **III** in vacuo and aqueous phase can be compared as above (see Figures S3 and S4).

For complex **I** in vacuo, the first singlet state is calculated by TDDFT at an energy as low as 0.71 eV, corresponding to a low-intensity (oscillator strength $f = 0.005$) absorption at 1758 nm. It accounts for a ligand-to-bipyridine charge transfer, where it involves an important charge redistribution. However, its low energy results from the unreasonably too small HOMO–LUMO gap. Similar low-lying LLCT states have already been reported as an artifact of TDDFT²⁸ due to an underestimation of the energies of long-range CT.²⁹ In the infrared and red regions, the spectrum simulated for the isolated molecule presents an unrealistic low-energy absorption band, ranging from about 600 to 900 nm, which is ILCT in character (electron transfers from the imidazole phenyl fragment to the phenanthroline). In contrast, no absorptions are calculated above 600 nm in solvent media. The lowest energy transition at 567 nm possesses both ILCT and LBCT characters (Table S6).

As for **II**, the absorption simulated around 460 nm in vacuo and 450 nm in H₂O is composed of both ILCT and MLCT transitions. On the basis of our theoretical calculations, a more detailed attribution of this rather large band evidences that the intraligand excitations dominate on the low-energy side, the ruthenium-to-bipyridine ones (MBCT) in the middle, and the ruthenium-to-phenanthroline ones (MPCT) in the high-energy side (Table S6 and Figure S3).

For **III**, the determined HOMO–LUMO gap is larger than 3 eV in vacuo as well as in solvents. Consequently, no absorption is calculated at wavelengths larger than 500 nm, whatever the surroundings. However, as the energy gap of vacant orbitals of bpy and phen shrinks in solvents compared to that in vacuo, the simulated spectrum in the metal-to-ligand region presents two separated bands for the isolated molecule (~450 nm, essentially MPCT absorptions, and ~400 nm, essentially MBCT

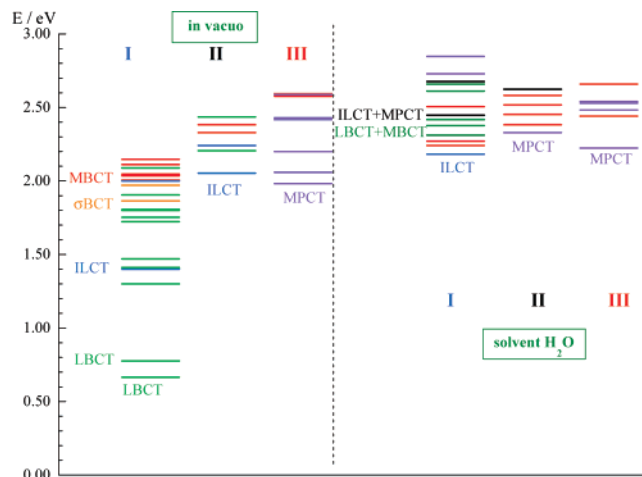


Figure 7. Lowest triplet states calculated by TDDFT on the ground-state geometries of the isolated molecule both in vacuo (left) and in water (right) for the complexes **I**, **II**, and **III**.

absorptions), which collapse around 430 nm in H₂O (Figure S4 and Table S7). Low-intensity intraligand transitions are calculated around 380 nm in vacuo and are carried to higher energy in water, owing to the stabilization of the ligand orbitals in polar media.

To sum up, energies calculated in vacuum by TDDFT for ligand-to-bipyridine (compound **I**) as well as intraligand charge-transfer transitions (compound **I** and **II**) are underestimated. Such excitations involve an important electronic migration from one part of the molecule to another one. Other authors have previously pointed out such phenomenon.^{5,29} On a theoretical basis, it originates from the so-called self-interaction error inherent to the DFT method²⁹ and depends strongly on the functional used.³⁰ Inclusion of exact Hartree–Fock exchange by using a hybrid functional (such as B3LYP) improves the results. Some tests on the choice of the functional are reported in the discussion section.

It has also been shown that inclusion of the solvent surrounding leads to a better description of the spectra.^{4,5} Indeed, our results confirm that such charge-transfer transitions are shifted to higher energy in polar solvents. A convincing piece of evidence is given in Figure 4 for compound **I** (and to a less extend in Figure S1 for **II**). As the polarity of the solvent increases, all of the orbitals developed on the electron-rich ligand L are stabilized by comparable amounts relative to the bpy or ruthenium orbitals. This is true for occupied as well as vacant orbitals. On each fragment of the molecule, the MOs are effected by the solvent in a similar manner; however, each moiety may behave differently. This explains why charge transfers involving different parts of the complex are strongly effected. As the d_{π} and bpy orbitals experience, in a similar manner, the presence of the solvent, MBCT transitions are only slightly effected. The influence on MPCT transitions is however more pronounced.

Excited Triplet States. All triplet T_n states lying at an energy smaller than the excitation energy used in the photophysical experiments ($\lambda_{\text{exc}} = 440$ nm) are susceptible to play a role in the deactivation processes. Therefore, the triplet states of low energy of the three complexes are calculated by TDDFT (in the optimized geometry of the ground state) both in vacuo and in solvent. The results are collected in Table S8 for the isolated molecule and Table S9 for the water solution. The important modifications, which result from calculations in these two different media, are clearly evidenced in Figure 7. As expected, trends previously discussed for the singlet states also hold for the triplet ones, when the in vacuo data are compared

to those obtained in solution. The results in the two media are less different when the electron density on the imidazole ring decreases.

For **I**, several states are calculated for the isolated molecule at very low energy (T_1 at 0.7 eV). They involve electron shifts from the imidazolate moiety (LBCT or ILCT). As discussed above, due to the calculation method, they are not relevant to the experimental data. The lowest metal-to-ligand charge transfer state is calculated as the 15th state and results from a transfer from the metal to bipyridine (MBCT). PCM calculations lift the energies of LBCT and ILCT states by at least 1.5 eV so that in water, only one such state (essentially ILCT character) is obtained at 2.18 eV, a value which is close to the first ruthenium-to-ligand charge transfer state (MBCT state at 2.24 eV). Interestingly, it is to be noticed that the transitions from the ruthenium orbitals are only slightly shifted to higher energy in solution, as compared to that in vacuo.

For complex **II**, results in vacuo are more pertinent even if four ILCT or LBCT states are found at energy lower than the first MLCT state; indeed, T_1 is calculated at 2.05 eV in the ground-state geometry. In H_2O , the lowest triplets are metal-to-ligand charge transfer in character, and T_1 lies at 2.33 eV. Here too, the ILCT monoexcitations remain present in the same energy range.

The computed data for **III** indicate that, concerning the compound with protonated imidazole, changes between the isolated molecule and the molecule in solvent surroundings are small. Both in vacuo and in H_2O , the lowest triplets are metal-to-phenanthroline charge-transfer states, and T_1 is calculated at 1.98 and 2.23 eV for the isolated molecule and in water, respectively.

The collected data in this section already pave the way, at least on a qualitative basis, for the interpretation of our photophysical properties; the use of computations on the isolated molecule may be correct for complex **III** but will give misleading derivations for compound **I**. This will be developed later after the direct study of two states involved in photophysics.

Lowest Triplet State and Oxidized Complexes. As photophysical experiments (without or with an electron acceptor) may involve the lowest triplet state T_1 of each complex as well as the ground doublet state D_0 of the oxidized forms, we now focus on our results both in vacuo or in a condensed phase. For each compound, T_1 was first investigated in vacuo using spin-unrestricted UB3LYP/LanL2DZ calculations followed by geometry optimization. Single point calculations using this geometry were then performed with the PCM model in different solvents. The same procedure was followed for the ground-state D_0 of the oxidized complexes. The prominent theoretical outcomes are reflected on the spin density distributions, which allow one to define the electronic map of the states. They can be visualized for the T_1 and D_0 states of the three complexes in Figure 8 for the in vacuo calculations and in Figure 9 for those in aqueous surroundings. As can be seen, the labels of the states are the same in both media for the complex with protonated imidazole, while discrepancies are found for complexes **I** and **II**. Consequently, calculations on the isolated molecule are suspected to afford erroneous results in the interpretation of their photophysics.

Complex II. An elegant way to describe the electronic redistribution occurring upon triplet formation is to examine the energy correlations between the (spin) orbitals in the three states. Such a diagram calculated in water is presented in Figure 10 for **II**. The energies of the occupied orbitals developed on the imidazole phenyl and phenyl part are only slightly modified

upon going from S_0 to T_1 . In contrast, the α -vacant $\pi_1^*(bpy)$ is stabilized and acts as the acceptor for an electron, while the highest d_π spin orbital with β spin rises in energy and is therefore depopulated. Thus, the lowest triplet state is generated by promotion of an electron from $d_\pi(Ru)$ to $\pi_1^*(bpy)$, that is, through a metal-to-bipyridine charge transfer (MBCT). Its energy is calculated as 2.18 eV above the ground state (each state in its own optimized geometry). This value corresponds to an emission wavelength of 569 nm for a deactivation toward the ground state. In water, the lowest triplet state, calculated by TDDFT at the geometry of the in vacuo ground state, is MPCT in character, lying at 2.33 eV. The energy diagram also points out that the metallic spin orbitals (except the β LUMO) are stabilized (mean value ~ 1.5 eV), which indicates that ruthenium is now in a higher oxidation state (virtually Ru^{III}) as a consequence of the electron transfer. The resulting spin density distribution (Figure 9) shows that approximately one spin is located on the ruthenium while the other is distributed over the two coordinated bipyridines. This 3MBCT state is a charge separated state.

The energy level diagram for the doublet ground state of the oxidized $[Ru(bpy)_2(PhenImHPh)]^{3+}$ complex (**II_{ox}**) in water is reported in the right part of Figure 10. A comparison with the triplet state shows important changes. The occupied α $\pi_1^*(bpy)$ spin orbital rises in energy and is hence depopulated as in the ground state, while the β LUMO is still a d_π spin orbital. This expresses that the oxidation has occurred on the ruthenium ion, which remains formally Ru^{III} , that is, D_0 is a 2MC (metal-centered) state. We remark that all of the occupied spin orbitals which are developed on L (localized on imidazole, on a phenyl ring, or on phenanthroline, as well as delocalized) retain (after leveling) the same energy in water in all three states. They are precisely involved neither in the excitation to the lowest triplet nor in the oxidation process.

As discussed above for the ground states, orbitals developed on the electron-rich imidazole part are calculated in vacuo at an energy too high relative to other MOs because the absence of a surrounding medium prevents the stabilization of the accumulated charges. This holds for the other states. In consequence, the energy correlations in vacuo between the (spin) orbitals in the three states (Figure S5) allow one to understand that D_0 is calculated as a 2LC (ligand-centered) state.

Complex I. The correlation diagram between MOs in S_0 , T_1 , and D_0 in water is reported in Figure S6. What has been emphasized for **II** is, a fortiori, true for **I**; in vacuo, an orbital developed on the deprotonated imidazole phenyl moiety is calculated as the HOMO in all states and is responsible for the 3LBCT and 2LC states.

As shown in Figure 4, solvent effects exert drastic changes on the MO levels. In order to more precisely understand the origin of the discrepancy in the nature of the T_1 states between the 3LBCT calculated in vacuo and the 3MBCT calculated in water, we have extended the study of the S_0 and T_1 to two other media, CH_3CN ($\epsilon = 36.6$) and CH_3OH ($\epsilon = 32.6$). Some results are compared in Table S10. T_1 rises in energy as the dielectric constant of the solvent increases, but without direct correlation. The compelling statement is that vacuum and water solution represent the two utmost surroundings acting on a molecule comprising an electron-rich moiety and generating, respectively, the 3LBCT and 3MBCT lowest triplets described above. In media of intermediate polarity, T_1 exhibits a mixing of 3LBCT and 3ILCT character, as pointed out by the spin density distribution calculated in CH_2Cl_2 and presented in Figure 11. With the increasing solvent polarity, the states generated from the ground

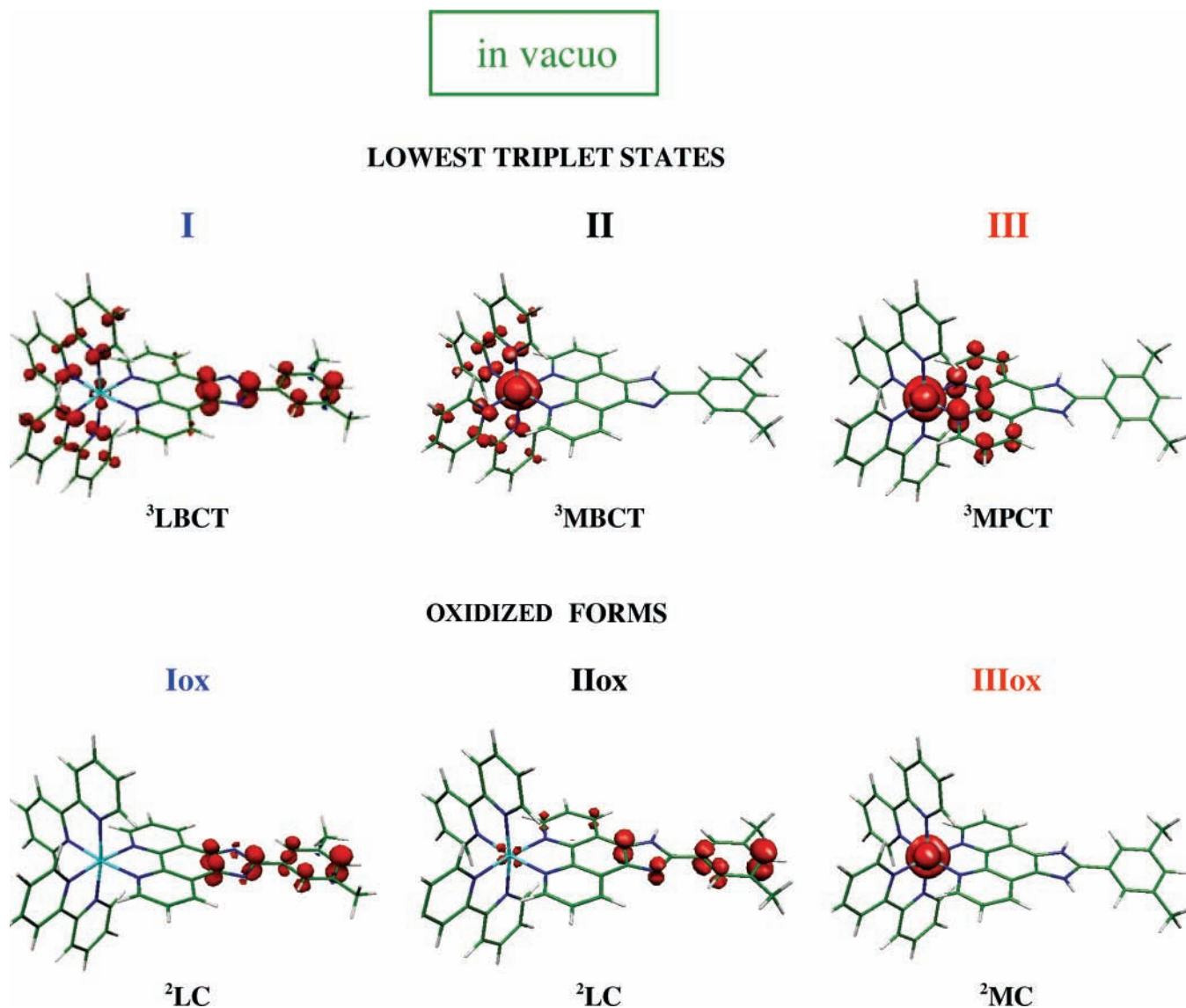


Figure 8. Spin density distribution for the lowest triplet state T_1 and the oxidized form D_0 of the three complexes calculated in vacuo.

state by a long-range ligand–ligand excitation increase in energy. This holds, to a less extent, for imidazole phenyl-to-phenanthroline ILCTs. A metal-to-ligand charge transfer which involves the inner part of the molecule becomes the lowest triplet in a highly polar solvent; however, in water, the lowest $^3\text{LBCT}$ lies only 0.13 eV higher than $^3\text{MBCT}$ (Table S10). These findings reproduce the trends obtained in TDDFT calculations (Figure 7). Nevertheless, care must be taken in the generalization of this comparison. Theoretical justifications assert the conclusion for the TDDFT method²⁹ on the ground-state geometry. However, oversimplifications underlie the present observation; in effect, the DFT/PCM calculations of S_0 and T_1 in different solvents are performed at the corresponding optimized geometry of the isolated molecule.

Complex III. Owing to the relatively small changes observed on the MO diagram of **III** in all solvents, the agreement between the states calculated in vacuo and in water is not surprising. As found for the UV–vis spectrum, in all media, the lowest triplet results from a HOMO–LUMO excitation ($^3\text{MPCT}$ state). The oxidized state results from the removal of an electron in the HOMO (^2MC state). The correlation diagram between S_0 , T_1 , and D_0 in water is reported in Figure S7.

Thereby, we point out that calculations in the absence of solvent can lead to reliable interpretations only for complex **III**,

in which no important heterogeneity in the charge distribution is present. We conclude that whatever the medium, the D_0 state results from an electron abstraction from the HOMO of the ground state. In contrast, the nature of the T_1 state cannot be predicted a priori from the MO diagram.

Discussion

Density functional analysis is taking a prominent part in coordination chemistry, this in view to bring a more detailed understanding of both the physical properties and reactivity patterns of metal complexes. DFT calculations are now commonly used for low-molecular-weight complexes but are both timely and intrinsically limited for more elaborate systems. In our laboratories, we are involved in a research program concerning photoinduced electron-transfer studies using chromophores such as ruthenium(II) polypyridine complexes. In order to interpret our experimental photophysical data, we have found that DFT calculations can be a valuable asset for us. However, to tackle such a task, it seems crucial to clarify the appropriate methodologies used in our research and bring further comparison toward other available ones. This comparative approach is an important criterion to argue for the choice of the functionals and the presence or not of the solvent medium. Below, we discuss these points.

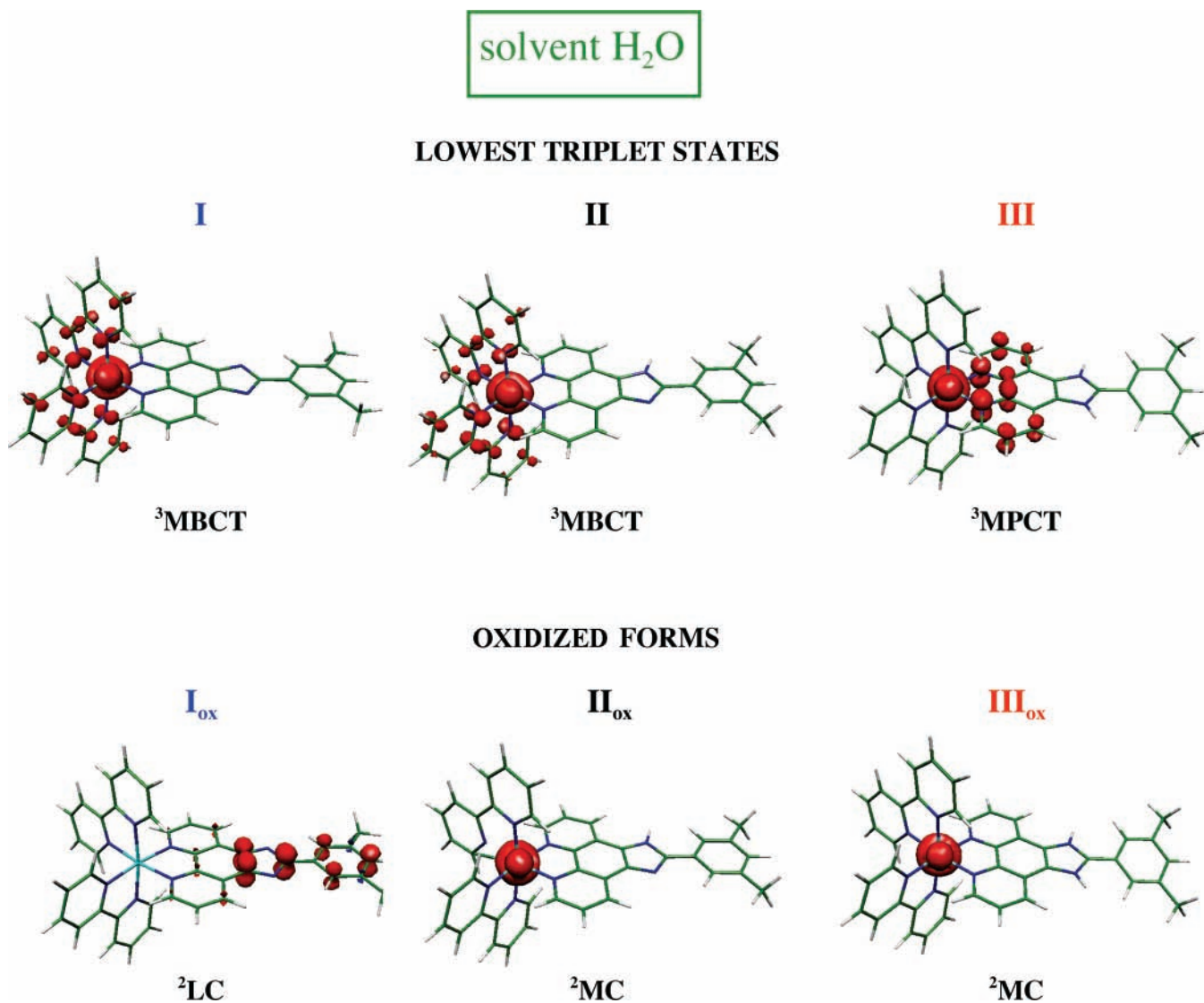


Figure 9. Spin density distribution for the lowest triplet state T₁ and the oxidized form D₀ of the three complexes calculated in water.

Choice of the Functional. Intrinsically in DFT calculations, the exchange–correlation functional is approximate. However, an in-depth discussion of the choice of the functional is far over the scope of this work. A part of *A Chemist’s Guide to Density Functional Theory*³¹ is devoted to the quest for approximate exchange–correlation functionals, and the general resulting conclusion is that functionals such as BP86, BLYP, or B3LYP are still the mainstay in most chemical applications. As for transition-metal complexes where electronic correlation plays an important part, the B3LYP functional seems to be a good choice.^{26,32} Geometry optimizations at the B3LYP/LanL2DZ have been indeed performed with success for ruthenium polypyridine-type complexes, but often with fewer atoms (for instance with a bpy replaced by two NCS[−] groups).³³ Other functionals such as PBE0³⁴ have been used in similar calculations.^{35,36} Surprisingly, there are few comparative works dealing with excited states involved in UV spectra or photophysics. For instance, Fantacci et al.,²⁵ in a comparison of the ability of the two functionals PBW91 and LB94 to reproduce the electronic spectrum of [Ru(4,4′-COOH-2,2′bpy)₂(NCS)₂], drew the conclusion that it is difficult to argue in favor of one functional over the other.

It is known that TDDFT yields errors in the excitation energies of charge-transfer states^{29,30,37} and that better accuracy is reached by using hybrid functionals which include a mixture

of exact Hartree–Fock exchange with DFT exchange correlation. Consequently, changes in the ratio of HF/DFT exchange may affect the results. Zalis et al.³⁰ have compared the dependence of the TDDFT transition energies on the amount of HF exchange in [Ru(X)(Me)(CO)₂(α-diimine)] complexes. The concluding remarks are (i) XLCT transitions are more sensitive than MLCT ones and (ii) pure functionals (0% HF exchange) strongly underestimate the transitions energies while they are overestimated by functionals containing more than 50% HF exchange. The best agreement with experiment was reached with the functional PBE1PBE (also called PBE0 with 25% HF exchange).

It is difficult to draw an unequivocal conclusion because modeling of the solvent in calculations also shifts the low-lying CT transitions to higher energy.⁵ In order to reproduce the electronic spectra of [Re(Cl)(CO)₃L] complexes in which long-range LLCT transitions are involved, HF exchange in both the functional and solvent reaction field were included.^{1,6}

We have chosen [Ru(bpy)₃]²⁺ for testing the above methodologies using three hybrid functionals, (i) B3LYP proposed by Becke,¹³ which includes 23% of Hartree–Fock exchange, (ii) PBE1PBE, the hybrid functional of Perdew, Burke, and Ernzerhof,³⁸ which uses 25% exchange and 75% correlation weighting, and (iii) BHandHLYP,¹³ which contains 50% of Hartree–Fock exchange. DFT calculations in vacuo were carried

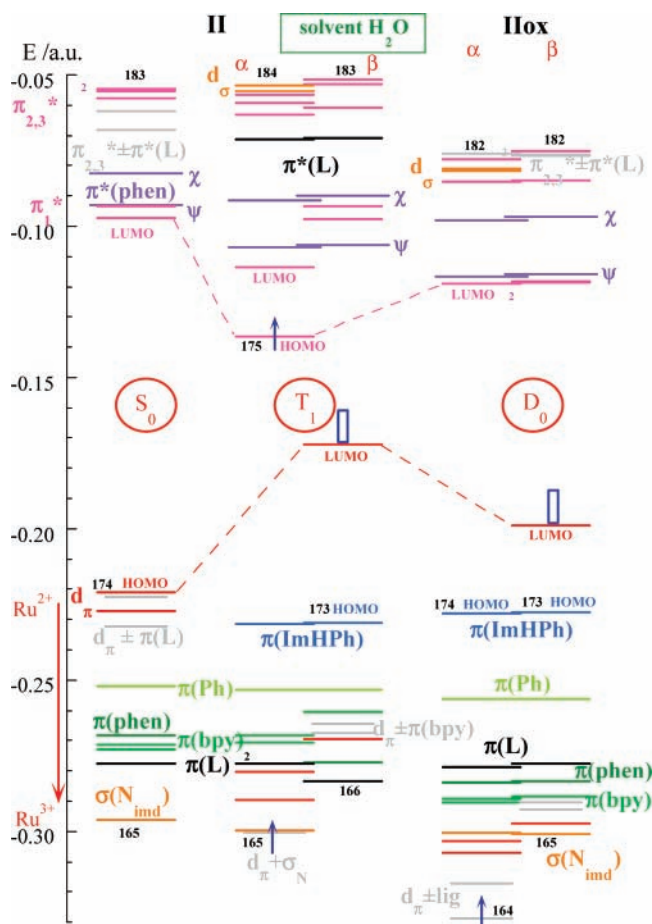


Figure 10. Energy level diagram (in au) of frontier orbitals calculated in H₂O for **II** in the ground-state S₀ (left) and in the lowest triplet state T₁ (middle) as well as for the D₀ ground state of the oxidized complex **IIox** (right) without leveling. Orbitals resulting from important mixing are drawn in gray. The blue arrows indicate the approximately uncompensated α spins.

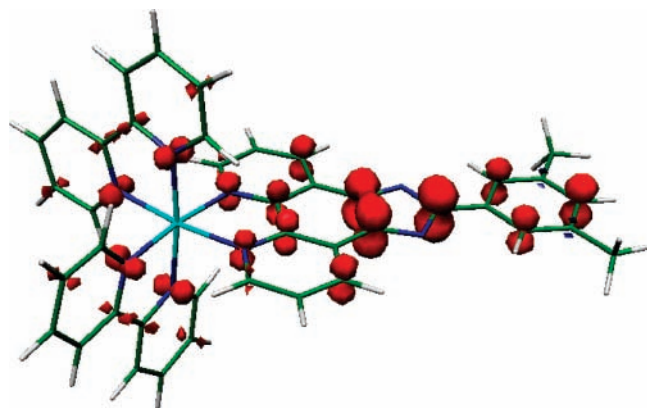


Figure 11. Spin density distribution for the lowest triplet state T₁ of **I** calculated in CH₂Cl₂, evidencing a mixing of LBCT and ILCT characters.

out using these functionals along with the previous basis set LanL2DZ, and geometry optimizations were performed in *D*₃ symmetry. We have found that the calculated geometric parameters changed only slightly. However, distinctive differences in the energies of the MOs were computed, as reflected by the values of the HOMO–LUMO gaps which are 6.06 and 3.76 eV with the BHandHLYP and PBE1PBE functionals, respectively, in comparison with 3.36 eV⁹ using the B3LYP one.

As a matter of fact, BHandHLYP can be discarded as it gives irrelevant excited states at too high energy. To compare the two other functionals, the lowest excited singlets were calculated by TDDFT in vacuo, and the corresponding UV–visible spectra were simulated (Figure S8). With PBE1PBE, the first transition was calculated at 2.69 eV (461 nm), and the intense ($f = 0.120$) MLCT transition at 3.05 eV (406 nm) was compared to 2.52 eV (492 nm)⁹ and 2.89 eV (430 nm; $f = 0.109$), respectively, with B3LYP. Experimentally, the MLCT transition was observed close to 450 nm in different solvents.^{39,40} Hence, on the basis of only this limited aspect of the absorption spectrum, B3LYP seems more adapted over PBE1PBE. We must emphasize that more elaborated comparisons between calculated and experimental data, especially to test the description of triplet states, would be necessary. We also notice that no solvent effect was taken into account. From these, our choice was guided toward B3LYP throughout this study.

Comparison with Ruthenium Tris(bipyridine) in Solvent Media. The most common criticism to the use of DFT methods is the absence of a solvent medium in the calculation procedures. Therefore, it is important to infer in which case it is mandatory to include solvent effects to obtain low-lying excited states with reliable energy and character. B3LYP/PCM calculations of [Ru-(bpy)₃]²⁺ have been performed in CH₂Cl₂ and H₂O, and the resulting MO diagrams have been compared with that obtained for the isolated molecule (Figure S9). Aside from the global destabilization in polar solvents, all energy gaps remain the same. It is then not surprising that calculations on the isolated molecule give reliable conclusions on the excited-state properties in solvent, as already pointed out.⁹ Ruthenium tris(bipyridine) can be conceptualized as a spherical molecule, with no heteroatom at the periphery, and is almost unaffected by the surrounding. This is however only true as long as solvent fluctuations are not taken into account. Indeed, this statement no longer holds for the complexes studied here, where an elongated ligand bears an imidazole group which is susceptible to charge variations and is easily accessible to solvent molecules.

Conclusion

In this paper, we have investigated the influence of a model surrounding on the calculated ground- and low-lying excited-state properties of ruthenium polypyridine complexes. For this purpose, comparison has been made between the DFT and TDDFT results obtained on the isolated molecule and in solvents of different polarity described in the framework of the polarized continuum model. The interesting point is that the study was performed on three closely related molecules which are iso-electronic and differ only by the protonic state of the main ligand. In such a situation, the influence of any important geometric changes is avoided, and the main factor to consider is the change of charge of the ligand, that is to say, an imidazolate, imidazole, or imidazolium fragment.

Calculations in the absence of surroundings have proven to give erroneous conclusions for the MO description of the ground state as well as for the energy and nature of the low-lying states for the complex with the electron-rich imidazolate (compound **I**). On the other side, after comparison of the results in all media, it emerges that, for the complex with positively charged imidazolium (compound **III**), the data calculated in vacuo already corroborate the experimental UV–visible spectrum as well as the photophysical properties. The situation is mitigated for the complex with normal imidazole (compound **II**). Indeed, the influence of solvent seems to be most important for calculations of polarizable mixed-ligand complexes.¹ This is

especially true when the highest occupied orbitals are developed on an external part of the molecule (as exemplified here for the imidazole phenyl moiety) and are involved in transitions to low-lying states.

The fact that DFT calculations on the isolated molecule result in a small HOMO–LUMO gap for the singlet ground state in such a family of complexes evidences that calculations in a model medium are absolutely mandatory to interpret experimental data. However, we do not have, to date, a general a priori recipe to avoid time-consuming calculations in solvent.

Acknowledgment. This work was supported by the CNRS (ANR Blanc HYPHO). We thank the Centre Informatique National de l'Enseignement Supérieur at Montpellier (France) and the Institut du Développement et des Ressources en Informatique Scientifique at Orsay (France) for providing calculation means.

Supporting Information Available: Supplementary figures and tables which have been mentioned in the text. This material is available free of charge via the Internet at <http://pubs.acs.org>.

References and Notes

- Vlcek, A., Jr.; Zalis, S. *Coord. Chem. Rev.* **2007**, *251*, 258.
- Stoyanov, S. R.; Villegas, J. M.; Rillema, D. P. *Inorg. Chem. Commun.* **2004**, *7*, 838.
- Villegas, J. M.; Stoyanov, S. R.; Huang, W.; Lockyear, L. L.; Reibenspies, J. H.; Rillema, D. P. *Inorg. Chem.* **2004**, *43*, 6383.
- Fantacci, S.; De Angelis, F.; Sgamellotti, A.; Re, N. *Chem. Phys. Lett.* **2004**, *396*, 43.
- Vlcek, A., Jr.; Zalis, S. *J. Phys. Chem. A* **2005**, *109*, 2991.
- Gabrielsson, A.; Matousek, P.; Towrie, M.; Hartl, F.; Zalis, S.; Vlcek, A., Jr. *J. Phys. Chem. A* **2005**, *109*, 6147.
- Villegas, J. M.; Stoyanov, S. R.; Huang, W.; Rillema, D. P. *J. Chem. Soc., Dalton Trans.* **2005**, 1042.
- Quaranta, A.; Lachaud, F.; Herrero, C.; Guillot, R.; Charlot, M.-F.; Leibl, W.; Aukauloo, A. *Chem.—Eur. J.* **2007**, *13*, 8201.
- Charlot, M.-F.; Pellegrin, Y.; Quaranta, A.; Leibl, W.; Aukauloo, A. *Chem.—Eur. J.* **2006**, *12*, 796.
- Pellegrin, Y.; Berg, K. E.; Blondin, G.; Anxolabéhère-Mallart, E.; Leibl, W.; Aukauloo, A. *Eur. J. Inorg. Chem.* **2003**, 1900.
- Lachaud, F.; Quaranta, A.; Pellegrin, Y.; Dorlet, P.; Charlot, M.-F.; Un, S.; Leibl, W.; Aukauloo, A. *Angew. Chem., Int. Ed.* **2005**, *44*, 1536.
- Pellegrin, Y.; Quaranta, A.; Dorlet, P.; Charlot, M.-F.; Leibl, W.; Aukauloo, A. *Chem.—Eur. J.* **2005**, *11*, 3698.
- Becke, A. D. *J. Chem. Phys.* **1993**, *98*, 5648.
- Lee, C.; Yang, W.; Parr, R. G. *Phys. Rev. B: Condens. Matter* **1988**, *37*, 785.
- Dunning, T. H., Jr.; Hay, P. J. *Modern Theoretical Chemistry*; Plenum, New York, 1976; Vol. 3.
- Hay, P. J.; Wadt, W. R. *J. Chem. Phys.* **1985**, *82*, 270.
- Frisch, M. J.; Trucks, G. W.; Schlegel, H. B.; Scuseria, G. E.; Robb, M. A.; Cheeseman, J. R.; Montgomery, J. A., Jr.; Vreven, T.; Kudin, K. N.; Burant, J. C.; Millam, J. M.; Iyengar, S. S.; Tomasi, J.; Barone, V.; Mennucci, B.; Cossi, M.; Scalmani, G.; Rega, N.; Petersson, G. A.; Nakatsuji, H.; Hada, M.; Ehara, M.; Toyota, K.; Fukuda, R.; Hasegawa, J.; Ishida, M.; Nakajima, T.; Honda, Y.; Kitao, O.; Nakai, H.; Klene, M.; Li, X.; Knox, J. E.; Hratchian, H. P.; Cross, J. B.; Bakken, V.; Adamo, C.; Jaramillo, J.; Gomperts, R.; Stratmann, R. E.; Yazyev, O.; Austin, A. J.; Cammi, R.; Pomelli, C.; Ochterski, J. W.; Ayala, P. Y.; Morokuma, K.; Voth, G. A.; Salvador, P.; Dannenberg, J. J.; Zakrzewski, V. G.; Dapprich, S.; Daniels, A. D.; Strain, M. C.; Farkas, O.; Malick, D. K.; Rabuck, A. D.; Raghavachari, K.; Foresman, J. B.; Ortiz, J. V.; Cui, Q.; Baboul, A. G.; Clifford, S.; Cioslowski, J.; Stefanov, B. B.; Liu, G.; Liashenko, A.; Piskorz, P.; Komaromi, I.; Martin, R. L.; Fox, D. J.; Keith, T.; Al-Laham, M. A.; Peng, C. Y.; Nanayakkara, A.; Challacombe, M.; Gill, P. M. W.; Johnson, B.; Chen, W.; Wong, M. W.; Gonzalez, C.; Pople, J. A. *Gaussian 03*, revision D.02; Gaussian, Inc.: Wallingford, CT, 2004.
- Casida, M. E.; Jamorski, C.; Casida, K. C.; Salahub, D. R. *J. Chem. Phys.* **1998**, *108*, 4439.
- Tomasi, J.; Mennucci, B.; Cammi, R. *Chem. Rev.* **2005**, *105*, 2999.
- Mennucci, B.; Tomasi, J. *J. Chem. Phys.* **1997**, *106*, 5151.
- Tomasi, J.; Mennucci, B.; Cancès, E. *J. Mol. Struct.: THEOCHEM* **1999**, *464*, 211.
- Cancès, E.; Mennucci, B.; Tomasi, J. *J. Chem. Phys.* **1997**, *107*, 3032.
- Cossi, M.; Scalmani, G.; Rega, N.; Barone, V. *J. Chem. Phys.* **2002**, *117*, 43.
- Cossi, M.; Barone, V. *J. Chem. Phys.* **2001**, *115*, 4708.
- Fantacci, S.; De Angelis, F.; Selloni, A. *J. Am. Chem. Soc.* **2003**, *125*, 4381.
- Monat, J. E.; Rodriguez, J. H.; McCusker, J. K. *J. Phys. Chem. A* **2002**, *106*, 7399.
- Wu, J.-Z.; Guang, Y.; Chen, S.; Ji, L. N.; Zhou, J.-Y.; Xu, Y. *Inorg. Chim. Acta* **1998**, *283*, 17.
- Bossert, J.; Daniel, C. *Chem.—Eur. J.* **2006**, *12*, 4835.
- Dreuw, A.; Head-Gordon, M. *J. Am. Chem. Soc.* **2004**, *126*, 4007.
- Zalis, S.; Ben Amor, N.; Daniel, C. *Inorg. Chem.* **2004**, *43*, 7978.
- Koch, W.; Holthausen, M. C. *A Chemist's Guide to Density Functional Theory*, 2nd ed.; Wiley-VCH: Weinheim, Germany, 2002.
- Barolo, C.; Nazeeruddin, M. K.; Fantacci, S.; Di Censo, D.; Comte, P.; Liska, P.; Viscardi, G.; Quagliotto, P.; De Angelis, F.; Ito, S.; Grätzel, M. *Inorg. Chem.* **2006**, *45*, 4642.
- Nazeeruddin, M. K.; Péchy, P.; Renouard, T.; Zakeeruddin, S. M.; Humphry-Baker, R.; Comte, P.; Liska, P.; Cevey, L.; Costa, E.; Shklover, V.; Spiccia, L.; Deacon, G. B.; Bignozzi, C. A.; Grätzel, M. *J. Am. Chem. Soc.* **2001**, *123*, 1613.
- Adamo, C.; Barone, V. *J. Chem. Phys.* **1999**, *110*, 6158.
- Guillemoles, J. F.; Barone, V.; Joubert, L.; Adamo, C. *J. Phys. Chem. A* **2002**, *106*, 11354.
- Laine, P. P.; Ciofini, I.; Ochsenein, P.; Amouyal, E.; Adamo, C.; Bedioui, F. *Chem.—Eur. J.* **2005**, *11*, 3711.
- Gritsenko, O.; Baerends, E. J. *J. Chem. Phys.* **2004**, *121*, 655.
- Perdew, J. P.; Burke, K.; Ernzerhof, M. *Phys. Rev. Lett.* **1996**, *77*, 3865.
- Curtis, J. C.; Sullivan, B. P.; Meyer, T. J. *Inorg. Chem.* **1983**, *22*, 224.
- Seneviratne, D. S.; Uddin, M. J.; Swayambunathan, V.; Schlegel, H. B.; Endicott, J. F. *Inorg. Chem.* **2002**, *41*, 1502.